Minimum Perturbation Coordinates on SO(3)

Matthew Travers†, Ross Hatton*, and Howie Choset⋆

***Abstract*— Systems that use internal shape changes to control their orientation in space have interested the geometric controls community for some time. Examples include the classic problem of a falling cat and the more applied attitude control of satellites. The dynamics of these systems are dominated by conservation of angular momentum, which induces a set of constraints between changes in shape and spatial orientation. This relationship can be combined with Lie bracket theory to identify shape changes that produce desired net rotations. The major weakness of the Lie bracket approach is that it only works for relatively small-amplitude motions; these methods depend on a local linearization of the system dynamics, which breaks down as larger motions are considered. Recent work on a related problem, planar locomotion, has shown that this breakdown can be mitigated by identifying a set of *minimum perturbation coordinates* for the system; application of Lie bracket theory in the minimum perturbation coordinates allows these methods to be applied to a broader and more interesting class of shape changes. In this work, we bring the derivation of minimum perturbation coordinates to the space of three-dimensional rotations. We show that as a result, we are able to derive visual tools that provide the control designer intuition into selecting cyclic controllers for inertial systems in free flight. These tools are demonstrated on a minimal satellite model taken from the literature.**

I. Introduction

The geometric mechanics community has expressed interest in inertial systems [1], [2], [3] that manipulate their internal degrees of freedom in order to reorient during free flight. Classical example systems include the falling cat [2], [4] and satellite in orbit [1], [3], [5], [6]. Models for these systems can be combined with Lie bracketing theory [7] in order to design closed trajectories in the input control space that effect desired net rotations. The purpose of this work is to provide new insight into the design of these controllers in the space of three-dimensional rotations.

Inertial control of systems in the space of three-dimensional rotations is difficult for a number of reasons. One is that the space of three-dimensional rotations is globally nonlinear. In addition, for non-differential rotations, the order in which the rotations occur cannot be interchanged, i.e., the underlying structure of the space is noncommutative. Another difficulty is that configuration spaces for inertial systems are usually underactuated. This work develops tools which mitigate the inherent difficulties of working in the space of three-dimensional rotations to aid the design of cyclic controllers for underactuated systems.

†The Robotics Institute, Carnegie Mellon University, Pittsburgh, Pennsylvania 15213, mtravers@andrew.cmu.edu

*School of Mechanical, Industrial, and Manufacturing Engineering, Oregon State University, Corvallis, OR 97331, ross.hatton@oregonstate.edu

⋆The Robotics Institute, Carnegie Mellon University, Pittsburgh, Pennsylvania 15213, choset@cs.cmu.edu

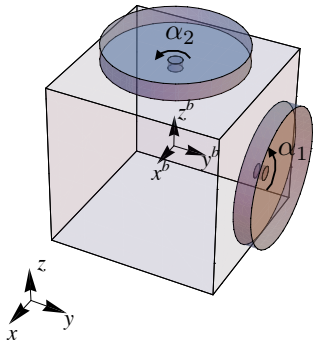

Fig. 1: Simplified model of a satellite. It is assumed without loss of generality that the origin of the inertial coordinate frame, (x, y, z), is co-located with the origin of the body-fixed coordinate frame, (x^b, y^b, z^b).

Previous reorientation control for inertial systems in free flight has largely focused on either computational or geometric methods. Computational approaches, which directly integrate a system's equations of motion, have shown success generating controllers over a large range of motions. The drawback of these methods is that they are often black box procedures which can potentially return poor solutions, such as those which take the system near or into a singularity, without incurring additional computational complexity. In addition, finding a *good* solution usually involves significant trial and error, as the quality of the solution is a function of the initial seed of the optimization procedure being solved.

On the other hand, geometric approaches leverage structure contained within the system model to provide valuable insight into local control design. For systems in free flight, this structure is contained within a linear relationship, derived from conservation of angular momentum, that maps shape changes to resulting orientation changes. Unfortunately, the linearity of this mapping is *only* a local property; it begins to break down as larger amplitude shape displacements are considered.

In recent work, Hatton and Choset [8], [9] addressed the local-linearity limitations, faced by previous geometric control design methods, in the space of planar rotations and translation. In [8], [9], the authors derive a set of coordinates, referred to as *minimum perturbation coordinates*, in which the effects of global nonlinearity as well as noncommutativity are mitigated. The benefit of the minimum perturbation coordinates is that they permit the use of geometric visualization tools [8], [9] to derive large amplitude cyclic shape-space controllers that produce desired position space locomotion. The minimum perturbation coordinates make available the

benefits of both geometric control, i.e., intuitive design, and computational methods, i.e., large amplitude displacements.

The main contribution of this work is providing a control designer with a set of visualization tools that allow them to intuitively design large-amplitude gaits for systems in the three-dimensioanl space of rotations. Viewed in non-minimum perturbation coordinates, these visualization tools are subject to the degradation of linearity in the mapping between shape and orientation changes; their effectiveness is thus limited to the design of small magnitude cyclic inputs. When viewed in the minimum perturbation coordinates, one can use the visualization toolset to design relatively large-amplitude cyclic inputs that even control unactuated degrees of freedom; we demonstrate the benefits of these tools on the satellite system shown in Figure 1.

The rest of this paper is organized as follows: A small review of relevant related work is presented in Section II. A brief analytical background of the geometric tools which form the foundation of this work is provided in Section III. The definition of minimum perturbation coordinates as well as their derivation on the three dimensional space of rotations is the subject of Section IV. An example which demonstrates the benefits of the minimum perturbation coordinates for inertial gait-based control is presented in Section IV as well. A discussion of results is provided in Section V. Conclusions and future work are presented in Sections VI and VII respectively.

II. Related Work

This work draws its origin from the locomotion literature developed by the geometric mechanics community. The work of Shapere and Wilczek [10], which studied locomotion in the framework of *gauge theory*, is largely viewed as the seminal work of geometric locomotion. Murray and Sastry [11], and then Kelly and Murray [12], dropped the explicit dependence on gauges, focusing more on the study of connections on principle bundles.

These early studies helped to lay out a rigorous mathematical framework for the study of locomotion. Fundamentally, the process by which internal shape changes affect locomotion via low level interaction with the surrounding environment was investigated. Two very important byproducts of this early research are the *reconstruction equation* and the *local connection*.

The reconstruction equation has been used to study a large number of locomotive systems with varied physical properties. For example, Walsh and Sastry examined linked rigid bodies reorienting [1] using the reconstruction equation. Ostrowski and Burrdick [7] used the reconstruction equation to examine a class of snake-like systems. Morgansen *et. al.* [13] used the reconstruction equation to study the locomotion of fish.

Several tools which leverage the geometric structure contained within the reconstruction equation have recently been developed. In the work of Hatton and Choset [9], *connection vector fields*, which visually represent the potential instantaneous changes in position due to changes in shape, were introduced. Shammas *et. al.* [14], used a combination of the reconstruction equation and Stokes Theorem to derive *height functions*, which serve as a tool for designing gaits resulting in specific motions of a three-link system with respect to its environment. Similar approaches have been adopted by Melli *et. al.* [15] as well as Avon and Raz [16].

III. Background

A brief background of the analytical components referenced in the rest of this paper are presented in this section. The derivations of these components are beyond the scope of this work, and as such are left to the noted references.

A. Kinematics

The rest of this paper focuses on configuration spaces, Q, that have the form $Q = \mathrm{SO}(3) \times M$, where $\mathrm{SO}(3)$ is a matrix *Lie group* which parameterizes the three-dimensional space of rotations, $\times$ is a group direct product, and M is the shape space. $\mathrm{SO}(3)$ is in this case the position space of Q.

In Section I, the underactuation of the configuration spaces of inertial systems was briefly discussed. Ordinarily, *desired* control is defined with respect to the system's orientation in $\mathrm{SO}(3)$, whereas the *available* control is over the shape, $r \in M$. Assuming complete control over the shape (which is a physically accurate assumption), we adopt the following notation, originally introduced in [9], in order to define the set of input control trajectories. A *shape change* is any trajectory in the shape space M. A *gait* ϕ is a cyclic trajectory in M which begins and ends in the same shape. The space of all gaits is denoted Φ. An *image family*, $\bar{\phi}$, is the set of all gaits that encircle the same region of M.

We would ultimately like to derive a relationship relating the set of potential shape controls to the resulting reorientation. In order to define this relationship, we start by taking $r = (\alpha_1, \alpha_2)$ and $g = (\theta_x, \theta_y, \theta_z)$ to be the parameterization of the shape and position spaces respectively. In the geometric literature, the relationship which relates position velocity, in terms of a *body velocity*, $\widehat{\xi} = R^T \dot{R}$ (where $\widehat{\cdot}$ is the hat operator which takes three dimensional vectors represented in $\mathbb{R}^3$ into the space of 3×3 skew-symmetric matrices and $R \in \mathrm{SO}(3)$ is a rotation matrix), to shape velocity, $\dot{r}$, is

$$\xi = -\mathbf{A}(r)\dot{r}, \tag{1}$$

where $\mathbf{A}(r)$ is the *local connection*, which in this paper is a 3×2 matrix. Equation (1) is the kinematic reconstruction equation [14]. In much the same way the manipulator Jacobian maps joint velocities into workspace velocities for robotic manipulators, the local connection maps shape velocities into position velocities for locomoting systems.

B. Connection Vector Fields

The kinematic reconstruction equation (1) analytically relates shape changes to reorientation in the world, but is only an effective computational tool when designing small amplitude shape motions or, once a large amplitude shape trajectory has *already* been selected. Equation (1) does not

by itself provide very much intuition into how different shape trajectories over a range of amplitudes effect reorientation.

Connection vector fields, originally identified by Hatton and Choset [17], provide a visual tool lending insight into how different shape velocities affect position-space velocities. A connection vector field is defined by treating each row of the local connection, $\mathbf{A}^i(r)$, as a vector field. The components of the body velocity can thus be viewed as the result of a dot product between the corresponding connection vector field and shape velocity,

$$\xi_i = \vec{\mathbf{A}}^{\xi_i}(r) \cdot \dot{r}. \tag{2}$$

Note that the minus sign in front of the local connection in (1) has been absorbed into the connection vector field components.

Adopting this vector field perspective lends itself to an interpretation which describes how connection vector fields map shape velocities into position velocities. The definition of a dot product states,

$$\xi_i = \vec{\mathbf{A}}^{\xi_i}(r) \cdot \dot{r} = ||\vec{\mathbf{A}}^{\xi_i}(r)||\ ||\dot{r}|| \cos\Theta, \tag{3}$$

where $||\vec{\mathbf{A}}^{\xi_i}(r)||$ and $||\dot{r}||$ are the magnitudes of the connection vector field and shape velocity, respectively, and Θ is the angle between them. Equation (3) offers geometric intuition into how shape changes affect displacements; the more aligned shape velocities are with the connection vector fields, the larger the displacement.

C. Constraint Curvature Functions

Connection vector fields illustrate the instantaneous relationship between shape and position changes, but do not directly convey information about the *net* change in position over a sequence of shape motions. Knowledge about such net motion plays a key part in understanding and controlling their behavior, as joint limits often force systems to use cyclic motions that include both forward and backward segments. The *curvature* of the local connection encodes useful information about this net displacement [10], which can be visually represented as a set of *constraint curvature functions* (CCFs) over the shape space [15], [16], which have also been referred to (for two-dimensional shape spaces) as *height functions* [14].

At an intuitive level, the CCFs are closely related to the curls of the rows of the local connection. By Green's form of Stokes' theorem [18], the line integral on a vector field along a closed loop is equal to the area integral of the field's curl over the interior of the loop. Taking this integral over a gait (a closed-loop path through the shape space) produces the *body velocity integral* (BVI), which represents the "forwards minus backwards" motion in each position direction, as observed from the body frame. The BVI does not fully capture the net displacement, however, because it discards the *order* in which the system moves in different position directions and the position space is not commutative. The CCFs restore some of this ordering information by augmenting the curl with a *local Lie bracket* term that measures the noncommutativity of the position space, producing a *corrected body velocity integral* (cBVI).

More precisely, the relationship between the cBVI and net displacement is given by an identity between the *exponential coordinates*[1] [15] $z(\phi)$ of the net displacement over a gait ϕ and a series whose first two terms correspond to the integral of the abstract *curvature* of the constraints over a region of the shape space bounded by ϕ [19]. This curvature is measured by the Lie bracket of the columns of the local connection, which measures the net translation induced by a differential oscillation in the system's shape. In two dimensional shape spaces, the identity appears as

$$z(\phi) = \iint_{\phi} \overbrace{\underbrace{-\text{curl}\mathbf{A}}_{\text{nonconservativity}} + \underbrace{\left[\mathbf{A}_1, \mathbf{A}_2\right]}_{\text{noncommutativity}}}^{\text{CCFs (full Lie bracket)}} dr + \text{higher-order terms}, \tag{4}$$

where the curl operator is applied individually to each row of $\mathbf{A}$, and $[\mathbf{A_1}, \mathbf{A_2}]$ is the *local* Lie bracket of the columns of $\mathbf{A}$ (taken as if $\mathbf{A}$ did not depend on the shape).

In (4), the curl term measures the *nonconservativity* of the local connection, or how the constraints change over the shape space, preventing antipodal segments of a stroke from pushing or pulling the system equally. The local Lie bracket and higher order terms correspond to the *noncommutativity* of the system's position space, i.e., the extent to which rotations do not commute.

For motions over which a system experiences little noncommutativity, the higher-order terms are small and the net displacement is closely approximated by the area integral of the first two terms in the equation (the system's CCFs). This makes it easy to characterize the locomotive capabilities of the system, in terms of the maximum displacement possible over any gait, and, as we discuss in the Section IV-B, to design useful gaits by simply encircling appropriate regions of the shape space. Historically, this condition of low noncommutativity was considered as only applying to small-amplitude gaits or certain special cases [15]. In recent work [9], [17], however, we have demonstrated a means for optimizing the coordinates to minimize the overall system noncommutativity and apply the CCF area rules to large-amplitude motion.

IV. Minimum Perturbation Coordinates on SO(3)

In Section I, the limitations of geometric control approaches due to the breakdown of local linearity was discussed. In addition, the notion of minimum perturbation coordinates, which were found to mitigate this problem in the space of planar rotation and translation, were also introduced. In this section, we derive the minimum perturbation coordinates on SO(3).

The minimum perturbation coordinates allow the geometric visualization tools described in Sections III-B and III-C to be more effective for designing gaits over a large

[1]The exponential coordinates of a rotation are the components of the constant body velocity required to reach that rotaion in unit time, starting from the origin.

region of the shape space. In Section IV-A we describe how the minimum perturbation coordinates minimize the position space motion induced by shape space control trajectories, effectively dampening the effects of intermittent shape motion during gait execution. An example which highlights several of the benefits afforded by the minimum perturbation coordinates is presented in the second portion of this section.

A. Minimum Perturbation Coordinates

In order to derive the minimum perturbation coordinate frame, we first define the space of all valid body frames. In previous work [8], [9], a valid body coordinate frame was defined to be a frame in which a local connection could be derived. The set of *all* valid body frames was shown to be equal to all frames related to a known-valid frame by a shape dependent transformation.

It is possible to define a quadratic cost function over the space of valid body-coordinate frames which can numerically be optimized to derive the minimum perturbation coordinates [8], [9]. Some intuition into how the quadratic cost is selected can be gained by referring back to (2). The rows of the local connection can be viewed as linear operators which map shape velocities into body velocities. This implies that the magnitude of the connection vector fields directly scale the effect that shape changes have on body-frame displacements. Minimizing the magnitude of the connection vector fields thus minimizes the effect that shape changes have on body-frame displacements. It is in this sense that we are deriving a minimum perturbation coordinate representation.

The optimization problem which yields the minimum perturbation coordinates can be posed as follows: given the connection vector fields represented in the original coordinates, $\vec{\mathbf{A}}^i_{\text{old}}(\cdot)$, determine the shape dependent transformation β which most nullifies the components of the connection vector fields in the new coordinates, $\vec{\mathbf{A}}^i_{\text{new}}(\cdot)$. While the exact meaning of "most nullifies" is open to interpretation, one choice of objective function is the sum of the average-squared magnitudes of the individual connection vector fields in the new body coordinates over a region Ω.

In previous work [8], [9], which considered systems in SE(2), this optimization was solved by applying a modified version of the discrete Hodge-Helmholtz decomposition, which was numerically solved via finite element methods. The same approach is adopted in this paper. The implementation details are left to the reference [9], although several important difference that occurs on SO(3) require further explanation.

In SE(2), the connection vector fields in the new frame, $\vec{\mathbf{A}}^i_{\text{new}}(\cdot)$, can directly be expressed as a linear combination of the connection vector fields in the old frame, $\vec{\mathbf{A}}^i_{\text{old}}(\cdot)$, and the transformation between the two frames, β_i. A linear relationship is *explicitly* required in order to implement the modified discrete Hodge-Helmholtz minimization [9]. In SO(3), no such direct linear relationship exists. Thus, in order to solve the coordinate optimization, we must first compute the linearization, about the shape, of the body velocity transformation between new and old frames.

We start by defining two valid body-coordinate frames, $(\theta^b_{x,\text{old}}, \theta^b_{y,\text{old}}, \theta^b_{z,\text{old}})$ and $(\theta^b_{x,\text{new}}, \theta^b_{y,\text{new}}, \theta^b_{z,\text{new}})$, related via the rotation matrix $R_\beta \in \text{SO}(3)$. Body velocities in the new frame, $\xi^{\text{new}} \in \mathbb{R}^3$, are related to body velocities in the old frame, $\xi_{\text{old}} \in \mathbb{R}^3$, by [20]

$$\xi_{\text{new}} = \text{Ad}_{g_\beta^{-1}} \xi_{\text{old}} + \xi_\beta, \tag{5}$$

where $\widehat{\xi}_\beta = R_\beta^T \dot{R}_\beta$ and $\text{Ad}_{g_\beta^{-1}}$ is the adjoint operator. In SO(3), $\text{Ad}_{g_\beta^{-1}} = R_\beta^T$, where R_β is a 3×3 rotation matrix. Thus, we can rewrite (5) as

$$\xi_{\text{new}} = \mathbf{R}_\beta^T \xi_{\text{old}} + \xi_\beta. \tag{6}$$

Noting that $R_\beta^T = \exp(-\widehat{\beta})$, where $\widehat{\beta}$ is an element of the tangent space at the identity element of the group, we make the first-order approximation $R_\beta^T \approx I - \widehat{\beta}$, where "$I$" is a 3×3 identity matrix. Next, using "hat" notation,

$$\begin{aligned}
\widehat{\xi}_\beta &= R_\beta^T \dot{R}_\beta \\
&= R_\beta^T \frac{\partial R}{\partial \widehat{\beta}} \dot{\widehat{\beta}}(r) \\
&= \exp(-\widehat{\beta}) \frac{\partial}{\partial \widehat{\beta}} \exp(\widehat{\beta}) \dot{\widehat{\beta}}(r) \\
&= (I - \widehat{\beta}(r) + \dots)(I + \widehat{\beta}(r) + \dots) \dot{\widehat{\beta}}(r) \\
&\approx \dot{\widehat{\beta}}(r),
\end{aligned} \tag{7}$$

where in the last line we are making a first-order approximation with respect to shape r. Rewriting (7) in vector notation, i.e., $\xi_\beta \approx \dot{\beta}$, and substituting in our approximation for R_β^T, (6) can be rewritten as,

$$\begin{aligned}
\xi_{\text{new}} &\approx \left(I - \widehat{\beta}\right) \xi_{\text{old}} + \dot{\beta} \\
&\approx -\mathbf{A}_{\text{old}}(r)\dot{r} + \widehat{\beta}\mathbf{A}_{\text{old}}(r)\dot{r} + \nabla_r \beta(r)\dot{r} \\
&\approx \left(-\mathbf{A}_{\text{old}}(r) + \widehat{\beta}\mathbf{A}_{\text{old}}(r) + \nabla_r \beta(r)\right)\dot{r} \\
&\approx -\mathbf{A}_{\text{new}}(r)\dot{r},
\end{aligned}$$

where we have substituted in $\xi_{\text{old}} = -\mathbf{A}_{\text{old}}(r)\dot{r}$, which is a consequence of our assumption that the old frame is valid, and $\dot{\beta} = \nabla_r \beta(r)\dot{r}$, which is an application of chain rule.

Having derived this linearization, we can finally define the objective function which is optimized to derive the minimum perturbation coordinates on SO(3),

$$\begin{aligned}
J = &\int\int_\Omega ||\vec{\mathbf{A}}^{\xi_x} + \beta_z \vec{\mathbf{A}}^{\xi_y} - \beta_y \vec{\mathbf{A}}^{\xi_z} + \nabla\beta_x||^2 d\Omega \\
&+ \int\int_\Omega ||\vec{\mathbf{A}}^{\xi_y} - \beta_z \vec{\mathbf{A}}^{\xi_x} + \beta_x \vec{\mathbf{A}}^{\xi_z} + \nabla\beta_y||^2 d\Omega \\
&+ \int\int_\Omega ||\vec{\mathbf{A}}^{\xi_z} + \beta_y \vec{\mathbf{A}}^{\xi_x} - \beta_x \vec{\mathbf{A}}^{\xi_y} + \nabla\beta_z||^2 d\Omega.
\end{aligned} \tag{8}$$

In the finite element method approach which is used to numerically optimize (8), the β_i's are restricted to a class of weighed sum basis functions ρ [9], such that $\beta_x = \sum_i \rho_i e_i$, $\beta_y = \sum_i \rho_i f_i$, and $\beta_z = \sum_i \rho_i h_i$, where e_i, f_i, and h_i represent the associated weights. The necessary conditions

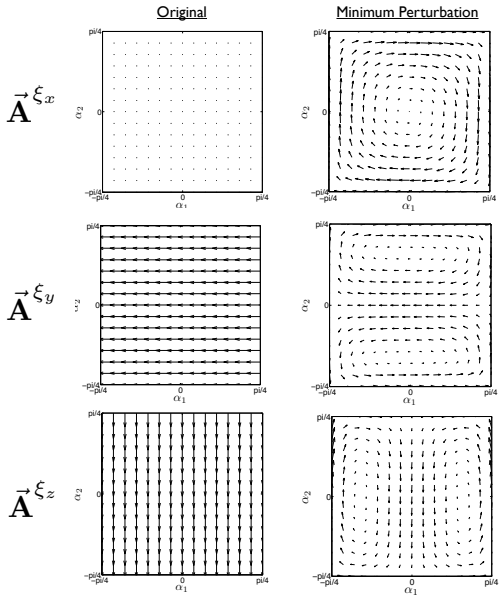

Fig. 2: Connection vector fields in the original as well as minimum perturbation coordinates.

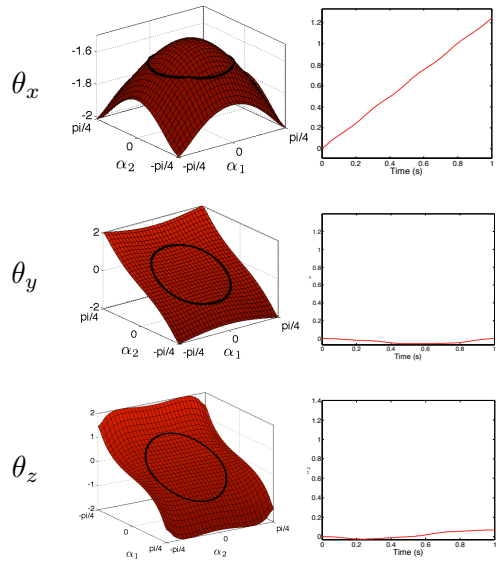

Fig. 3: CCFs in the minimum perturbation coordinates along with an example gait overlaid. The right column displays the resultant displacement in the position space due to executing the example gait.

for optimality, $\partial D/\partial e_i = 0$, $\partial D/\partial f_i = 0$, and $\partial D/\partial h_i = 0$ can then be used to generate the equated integrals

$$\int_\Omega \nabla\rho_i \cdot (\nabla\beta_x - \beta_z\vec{\mathbf{A}}^{\xi_y} + \beta_y\vec{\mathbf{A}}^{\xi_z}) + \rho_i(\beta_x\vec{\mathbf{A}}^{\xi_z}\cdot\vec{\mathbf{A}}^{\xi_z} - \vec{\mathbf{A}}^{\xi_z}\cdot\nabla\beta_y + \beta_x\vec{\mathbf{A}}^{\xi_y}\cdot\vec{\mathbf{A}}^{\xi_y} + \vec{\mathbf{A}}^{\xi_y}\cdot\nabla\beta_z) = \int_\Omega \nabla\rho_i\cdot\vec{\mathbf{A}}^{\xi_x}, \quad (9)$$

$$\int_\Omega \nabla\rho_i \cdot (\nabla\beta_y - \beta_z\vec{\mathbf{A}}^{\xi_x} + \beta_x\vec{\mathbf{A}}^{\xi_z}) + \rho_i(\beta_y\vec{\mathbf{A}}^{\xi_z}\cdot\vec{\mathbf{A}}^{\xi_z} + \vec{\mathbf{A}}^{\xi_z}\cdot\nabla\beta_x - \beta_y\vec{\mathbf{A}}^{\xi_x}\cdot\vec{\mathbf{A}}^{\xi_x} - \vec{\mathbf{A}}^{\xi_x}\cdot\nabla\beta_z) = \int_\Omega \nabla\rho_i\cdot\vec{\mathbf{A}}^{\xi_y}, \quad (10)$$

and

$$\int_\Omega \nabla\rho_i \cdot (\nabla\beta_z - \beta_y\vec{\mathbf{A}}^{\xi_x} + \beta_x\vec{\mathbf{A}}^{\xi_y}) + \rho_i(\beta_z\vec{\mathbf{A}}^{\xi_y}\cdot\vec{\mathbf{A}}^{\xi_y} - \vec{\mathbf{A}}^{\xi_y}\cdot\nabla\beta_x + \beta_z\vec{\mathbf{A}}^{\xi_x}\cdot\vec{\mathbf{A}}^{\xi_x} + \vec{\mathbf{A}}^{\xi_x}\cdot\nabla\beta_y) = \int_\Omega \nabla\rho_i\cdot\vec{\mathbf{A}}^{\xi_z}. \quad (11)$$

Defining a discretized grid on Ω, (9), (10), and (11) can be solved as a set of linear equations for the weights e, f, and h, thus deriving β.

In addition to having to derive the linearization of the relationship between connection vector fields in the new and old frames, we note here a second difference between the coordinate optimizations in SE(2) and SO(3). Deriving the minimum perturbation coordinates for SE(2) is a two step process. First, the minimum perturbation frame with respect to orientation is derived. Second, the minimum perturbation frame with respect to position is solved simultaneously for the body x- and y-coordinates (assuming $g = (x, y, \theta) \in$ SE(2)). The second optimization must be solved simultaneously for the body x- and y-directions because these two components are rotationally coupled. In SO(3), all three components of the position space are inherently coupled, and as such must simultaneously be optimized.

B. Example

In this section, we use the simplified satellite model shown in Figure 1 as an example to demonstrate the effectiveness of the minimum perturbation coordinates on SO(3). We assume that the satellite is free floating. We also assume that the origin of the world frame is co-located with the origin of the body frame. The system has direct control in the body y- and z-directions via gyroscopic actuators. The shape variables which parameterize these internal degrees of freedom are α_1 and α_2.

Figure 2, shows the connection vector fields represented in both the original and minimum perturbation coordinate frames. The coordinate optimization reveals some interesting information embedded within the vector fields. First, it appears that a class of nonintersecting gaits, $\Phi_{\text{sym}} \subset \Phi$, symmetric about the origin will cause net rotation in the θ_x direction. The intuition behind this comes from (3); any gait which symmetrically encircles the origin will have a net positive (or negative, depending on direction) dot product between shape velocities, the tangent at each point of the gait trajectory in shape space, and the connection vector field $\vec{\mathbf{A}}^{\xi_x}_{\text{new}}$. This is significant because in the original coordinates the connection vector field in the θ_x direction is equal to zero. The minimum perturbation coordinates thus provide insight into how motions for θ_x can be planned, where there is no such information available in the original coordinates. Secondly, the $\vec{\mathbf{A}}^{\xi_y}_{\text{new}}$ and $\vec{\mathbf{A}}^{\xi_z}_{\text{new}}$ connection vector fields also

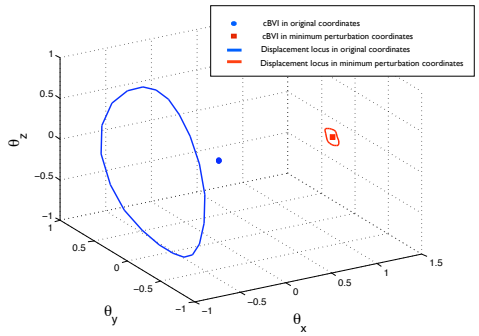

Fig. 4: cBVIs and displacement loci in the original and minimum perturbation coordinates.

reveal structures that are amenable to interesting gait execution. For example, again using (3) to guide our intuition, it appears that a figure-eight type gait which is symmetric about $\alpha_2 = 0$ can be designed to result in large amplitude θ_y displacements, with minimal θ_x and θ_z displacements.

To quantify the qualitative gait design analysis afforded by connection vector fields, the CCFs discussed in Section III-C can be plotted and analyzed. In previous work, Stokes' theorem was used to integrate the curl of connection vector fields over a region to calculate net displacements. In this paper, we note that this approach amounted to a first order approximation of the CCFs. CCFs integrate the curvature of the connection to calculate a higher-order estimate of net rotation. The CCFs along with an example gait, ϕ_{ex}, are plotted in Figure 3. The gait, ϕ_{ex} can be interpreted using the same *gait design rules* originally identified in [14]. These rules formalize intuition about position space displacement inferred from the value of the CCF over regions of the shape space encircled by a gait. For example, a gait which encircles a region of the shape space in which a CCF is sign definite will produce net motion in the associated component. A gait which encircles a region where a CCF function is equally positive and negative will produce zero net motion.

The gait shown in Figure 3 encircles a region of the CCF in the θ_x direction which is sign definite, and regions in the θ_y and θ_z directions where the CCF changes sign. According to [14] we would thus expect this gait to produce a nonzero displacement in the θ_x direction, as well as very little displacement in the θ_y and θ_z directions. The column on the right-hand side of Figure 3 displays the net group displacements which result from executing ϕ_{ex}. The displacements were calculated by numerically integrating the equations of motion for the satellite system. The displacement plots confirm that this gait does indeed result in a large magnitude displacement in the θ_x direction, and nearly zero displacement in both the θ_y and θ_z directions. Furthermore, if we abstract our view of gait execution to be the equivalent of flowing along an input control vector field for a discrete amount of time, i.e., one gait period, ϕ_{ex} provides nearly independent control of the θ_x position coordinate. This is interesting because the θ_x coordinate is not directly actuated. Even more interesting, using CCF analysis, it is clear that by changing the "radius" of a nonintersecting gait which is symmetric about the origin, it is possible to generate motions which produce arbitrarily large or small amplitude displacements of θ_x in the world. The class of nonintersecting gaits symmetric about the origin provide independent variable-amplitude control over an unactuated degree of freedom in the system.

V. Discussion

The minimum perturbation coordinates can be used by a designer to intuitively derive controllers in terms of gait-based behaviors for underactuated systems in $\text{SO}(3)$. There are several other major benefits afforded by gait design in the minimum perturbation coordinates: 1.) the minimum perturbation coordinates minimize the noncommutative effects of gait-based motions, 2.) in the minimum perturbation coordinates, the cBVI is an arbitrarily good approximation of net displacement, and 3.) the minimum perturbation coordinates capture the *net average motion* of a system executing a gait. Figure 4 provides an example which displays two of these benefits. In Figure 4, the red square represents the cBVI calculated in the minimum perturbation coordinates over the gait ϕ_{ex} in Figure 3. The red closed path around the square represents the displacement locus of the image family, $\bar{\phi}_{\text{ex}}$, related to ϕ_{ex}. The blue point in Figure 4 represents the cBVI calculated in the original coordinates, and the blue closed path the displacement locus associated with $\bar{\phi}_{\text{ex}}$, also calculated in the original coordinates. First, it is clear that the displacement locus for the image family $\bar{\phi}_{\text{ex}}$ in the original coordinates is much larger than the displacement locus in the minimum perturbation coordinates. Fundamentally, the difference in the displacement loci is due to the underlying noncommutativity of the group. Although overall, each member of the gait image family executes the exact same set of differential motions, the *order* in which they are executed is different for each member. The fact that the displacement locus calculated in the minimum perturbation coordinates is smaller than the displacement locus in the original coordinates implies that in the minimum perturbation coordinates there is much less sensitivity to the order in which the controller is executed. This can be interpreted by referring back to (4). The minimization of noncommutative effects in the minimum perturbation coordinates is equivalent to the minimization of the local Lie bracket in (4). Thus, in the minimum perturbation coordinates, CCFs are well approximated to the first-order.

It is important to note here that although the calculated position space rotations of the original and minimum perturbation frames are different in Figure 4, the overall *net rotation* is exactly the same regardless of coordinate choice. The difference of body frames is physically equivalent to a difference in initial conditions; the equations of motion are always the same, but the system's terminal configuration is a function of its initial configuration.

Second, in Figure 4, the cBVI calculated in the minimum perturbation coordinates is very close to the displacement locus also calculated in the minimum perturbation coordinates; much closer, relatively, than the cBVI and displacement locus calculated in the original coordinates. This is a visual

corroboration that the cBVI is a good approximation of net displacement in the minimum perturbation coordinates.

Finally, another benefit of the minimum perturbation coordinates is that they capture the net average motion of systems executing gaits. Intuitively, the minimum perturbation coordinates are derived by minimizing the effect that shape changes have on position displacements. As noted above, this is not to say that we have determined a coordinate set which changes how the system physically moves; the minimum perturbation coordinates simply dampen out the effects of intermittent-body motions that do not directly contribute to net position space displacement. This averaging effect is of particular interest for control designers interested in *very* large displacements, as they can focus their design on long-term macroscopic behavior without having to directly account for low-level oscillatory motions.

VI. Conclusion

This work derives a set of minimum perturbation coordinates on the space of three-dimensional coordinates. The benefits of doing so were shown to be that the minimum perturbation coordinates make available a set of visual geometric-design tools to the control designer. These tools make it possible to design closed-shape trajectories which affect desired net rotations. It was shown for the simplified satellite example that these tools could be used to design a gait which effectively provides independent control over the system's unactuated degree of freedom. It was also shown that the effects of noncommutativity are minimized when calculating net rotation in the minimum perturbation coordinate frame. Thus, calculating net rotation in the minimum perturbation coordinate frame, using only locally-linear information, provides a good estimate of net rotation in the nonlinear group.

VII. Future Work

Future work will largely focus on applying the gait design tools presented in Section III to systems which have more complicated relationships between shape and position space components than the satellite example system. This extension is of interest because the ideas presented in this work are particularly useful when designing controller for systems which possess singularities, both kinematic and mechanical. It most cases, it is difficult to design controllers which universally avoid singularities. Using the minimum perturbation coordinates presented in this work, it is possible to design a suite of gaits which produce specific position space locomotion while avoiding singularities. One such example system that we are considering is the Berkley Tailbot, which has shown remarkable progress in straight-forward PD-reorientation control. We are currently looking into gait design techniques for this system when the reorientation trajectories are aggressive enough that the current control scheme brings the mechanism into, and theoretically through, mechanical singularities.

In addition, we are also looking to extend this current work to further explore a minimum set of efficient gaits and high level planners which effectively link them together to produce complicated behaviors. This work will include examination of how to best define *efficiency*.

Acknowledgment

The authors would like to thank Evan Chang-Siu and Tom Libby for their insightful conversations which will ultimately lead the future direction of this research.

References

[1] G. Walsh and S. Sastry, "On reorienting linked rigid bodies using internal motions," *IEEE Transactions on Robotics and Automation*, vol. 11, no. 1, pp. 139–146, 1995.

[2] R. Montgomery, "Isoholonomic problems and some applications," *Comm. Math. Phys.*, vol. 128, pp. 565–592, 1990.

[3] Z. Li and L. Gurvits, "Theory and application of nonholonomic motion planning," Courant Inst. Math and Science, New York University, Tech. Rep., July 1990.

[4] R. Montgomery, *Gauge Theory of the falling cat*, ser. Dynamics nd Control of Mechanical Systems. American Mathematical Society, 1993.

[5] C. Byrnes and A. Isidori, "On attitude stabilization of rigid spacecraft," *Automatica*, vol. 27, pp. 87–95, 1991.

[6] Y. Nakamura and R. Mukherjee, "Exploiting nonholonomic redundancy of free-flying space robots," *IEEE Transactions on Robotics and Automation*, vol. 9, no. 4, pp. 499–506, 1993.

[7] J.Ostrowski and J. Burdick, "The mechanics and control of undulatory locomotion," *The International Journal of Robotics Research*, vol. 17, pp. 683–701, 1998.

[8] R. Hatton and H. Choset, "Optimizing coordinate choice for locomoting systems," in *Proceedings of the IEEE International Conference on Robotics and Automation*, Anchorage, AK, May 2010.

[9] ——, "Geometric motion planning: The local connection, stokes' theorem, and the importance of coordinate choice," *International Journal of Robotics Research*, vol. 30, no. 8, pp. 998–1014, 2011.

[10] A. Shapere and F. Wilczek, "Geometry of self-propulsion at low reynolds number," *Journal of Fluid Mechanics*, vol. 198, pp. 557–585, 1989.

[11] R. Murray and S. Sastry, "Nonholonomic motion planning: Steering using sinusoids," *IEEE Transactions on Automatic Control*, vol. 38, no. 5, pp. 700–716, 1993.

[12] S. Kelly and R. Murray, "Geometric phases and robotic locomotion," *Journal of Robotic Systems*, vol. 12, pp. 417–431, 1995.

[13] K. Morgansen, B. Triplett, and D. Klein, "Geometric methods for modeling and control of free-swimming fin-actuated underwater vehicles," *IEEE Transactions on Robotics*, vol. 23, pp. 1184–1199, 2007.

[14] E. Shammas, H. Choset, and A. Rizzi, "Geometric motion planning analysis for two classes of underactuated mechanical systems," *The International Journal of Robotics Research*, vol. 2007, no. 26, pp. 1043–1073.

[15] J. Melli, C. Rowley, and D. Rufat, "Motion planning for an articulated body in a perfect planar fluid," *SIAM Journal of Applied Dynamical Systems*, vol. 5, pp. 650–669, 2006.

[16] J. Avon and O. Raz, "A geometric theory of swimming: Purcell's swimmer and its symmetrized cousin," *New Journal of Physics*, vol. 9, 2008.

[17] R. Hatton and H. Choset, "Connection vector fields for underactuated systems," in *Proceedinds of the IEEE BioRobotics Conference*, Scottsdale, AZ, October 2008.

[18] W. Boothby, *An Introduction to Differentible Manifolds and Riemannian Geometry*. New York: Academic Press, 1986.

[19] J. Radford and J. Burdick, "Local motion planning for nonholonomic control systems evolving on principle bundles," in *Proceedings of the INternational Symposium on MAthematical Theory of Networks and Systems*, Padova, Italy, 1998.

[20] R. M. Murray, Z. Li, and S. Sastry, *A Mathematical Introduction to Robotic Manipulation*. CRC Press, 1994.